Microwave Review
December 2025, Vol. 31, No. 2, pp. 9-20
DOI: 10.18485/mtts_mr.2025.31.2.2

# Design and Fabrication of SRR-Loaded Cantor Fractal-Based Antenna Array with Mutually Coupled Fed Technique for Satellite Communication

Anuj Kumar Sharma, Vipul Sharma, Prateek Agarwal, Ashish Nainwal, Sanjay Singh

*Abstract* - **This study delineates the design, fabrication, and evaluation of a high-bandwidth component measuring 37.33 mm × 87.2 mm × 1.6 mm, a cantor fractal slotted defective ground surface (DGS) antenna array (1x2) for X-band (consisting of 8–12 GHz) and C-band (ranging from 4–8 GHz). A mutually coupled fed is employed to excite a patch antenna. A mutually coupled fed falls under the classification of a non-contact fed. Non-contact feeding systems can be engineered to reduce electromagnetic interference (EMI), especially in high-frequency applications. It also prevents impedance mismatches, hence enhancing bandwidth and gain. Defected ground surface (DGS) combined with a split ring resonator (SRR) enhances both gain and bandwidth. This research considers the fringing effect to ensure adequate separation between the feeding network and the patch. This study guarantees low mutual coupling and interference among patches while preserving a uniform radiation pattern. The operating bands of 7.05–8.53 GHz and 10.2–11.5 GHz are fully compatible with this architecture. The proposed antenna demonstrates favourable outcomes in both modelling and empirical measurement. It features an extensive impedance bandwidth of 1.48 GHz and 1.2 GHz with reflection coefficients ($S_{11}$) of -42.34 dB and -24.5 dB at resonance frequencies of 7.8 GHz and 10.7 GHz, respectively. This also attains a substantial gain of 10.05 dBi at 7.8 GHz, 7.95 dBi at 8.1 GHz, and 7.73 dBi at 10.7 GHz.**

*Keywords* - **Cantor fractal, Defected Ground Surface (DGS), Fringing Effect, Fractional Bandwidth (FBW), Mutually coupled fed, Split Ring Resonator (SRR).**

## I. INTRODUCTION

The term fractal was first introduced by B. Mandelbrot, who is widely regarded as the pioneer of fractal mathematics. The word originates from the Latin fractus, meaning “broken” or “irregular,” indicating structures that are self-similar and complex across multiple scales [1]. The application of fractal geometries in antenna engineering has revolutionized the way compact, multiband, and broadband antennas are designed. These geometries offer unique electromagnetic properties that are well-suited for modern wireless communication systems, where high data throughput and space efficiency are critical.

*Article history: Received January 03, 2025; Accepted October 13, 2025.*

Anuj Kumar Sharma, Vipul Sharma, Prateek Agarwal, Ashish Nainwal, and Sanjay Singh are with the Department of Electronics & Communication Engineering, Gurukul Kangri Deemed to be University, Haridwar, 249401, Uttarakhand, India. E-mail: anujsharma@gkv.ac.in, vipul.s@gkv.ac.in,prateek.aggrawal@gkv.ac.in, ashish.nainwal@gkv.ac.in, sanjay.singh@gkv.ac.in

Antennas are typically categorized based on their operational bandwidth into narrowband, wideband, ultra-wideband (UWB), and super-wideband types. Narrowband antennas, those with bandwidths less than 500 MHz, are often unsuitable for high-speed wireless communication. In contrast, wideband and UWB antennas, which operate above 500 MHz, offer significantly broader frequency coverage and are essential for multifunctional wireless systems.

An ultra-wideband antenna is characterized by its ability to support both narrowband and wideband operations. According to the Federal Communications Commission (FCC), the UWB spectrum for indoor and outdoor wireless communication spans from 3.1 GHz to 10.6 GHz [1, 2]. UWB technology allows the transmission of massive volumes of data through low-power, short-duration pulses, offering advantages such as low interference, high resolution, and high data rates.

Fractal antennas, known for their space-filling, self-similar structures, are widely utilized due to their compact size, lightweight nature, and multiband capabilities [3]. Numerous studies have investigated the implementation of fractal geometries to improve impedance bandwidth, radiation characteristics, and gain across multiple frequency bands. For example, when slot-loading techniques are integrated into UWB antennas, they facilitate the creation of multiple notch bands that suppress interference from neighboring narrowband systems such as WLAN (5.15–5.82 GHz), X-band (7.25–8.39 GHz), C-band (3.8–4.2 GHz), and WiMAX (3.3–3.6 GHz) [4–9].

Several notable works demonstrate innovative fractal antenna designs. Abdelaziz et al. proposed an inset-fed tri-band antenna on Rogers RT Duroid 5880 substrate for millimeter-wave and 5G applications, achieving a peak gain of 11.72 dBi at 38 GHz [10]. Similarly, Liu et al. introduced a dual-polarized, slotted, coaxially-fed antenna with high gain (8.6 dBi) at 5.2 GHz, employing U-slot geometries [11]. Kaur and Sharma developed an FR-4-based four-band antenna with 11.45 dBi gain at 8.72 GHz, supporting S-, C-, and X-band operations [12]. Other works include printed inverted-F antennas with dual-band, dual-sense circular polarization for 2.5 GHz and 3.5 GHz bands [13], reconfigurable designs using PIN diodes for dynamic narrowband/broadband switching [14], and CSRR-loaded multiband patch antenna arrays with high-gain performance [15]. Emerging technologies such as MIMO (Multiple-Input Multiple-Output) antennas are also gaining traction due to their spectral efficiency and high data capacity. In [16] and [17] are discussed the challenges and practical implementation of MIMO antennas, emphasizing their adaptability for compact wireless systems. Fractal miniaturization techniques have

 

further contributed to ISM band optimization at 2.4 GHz [18]. In recent research, advanced fractal antenna designs have addressed multiband functionality, enhanced radiation efficiency, and miniaturization. In [19] is developed a multiband fractal antenna for WiMAX, WLAN, C-, and X-bands, covering 2–12 GHz with high efficiency and stable radiation. In [20] is introduced a compact 34×34 mm² UWB-MIMO antenna with spiral coils and resonator slots to create effective WiMAX/WLAN notch filtering, yielding low ECC and high gain. In [21] is designed a 4-port fractal-SRR-based UWB-MIMO antenna with grounded stubs that achieved −25 dB mutual coupling and directional gain near 7.5 GHz. For millimeter-wave 5G (n258 band) applications, in [22] is proposed a spherical fractal MIMO antenna resonating between 9.5 and 26.6 GHz with >10 GHz bandwidth. In [23] is taken a futuristic approach, presenting a super-UWB quad-port fractal antenna operating up to 96 THz for 6G and terahertz communication. In [24] is presented a Koch-fractal DGS octagonal antenna resonating at 3.3, 6, and 8.6 GHz, exhibiting 96.8% radiation efficiency and 8.94 dBi gain at 12.25 GHz—suitable for WBAN/WPAN systems. In [25] is reported an aperture-coupled circular fractal UWB-MIMO antenna with complementary spiral DGS optimized for C-, Ku-, and satellite bands. Finally, in [26] is applied spline-based shape optimization using metaheuristics to engineer a compact 182 mm² UWB monopole with less than -10 dB reflection across the band, underscoring the trade-off between size and performance. These collective studies confirm that fractal-based UWB-MIMO antennas offer compelling solutions for compact, high-speed, and interference-resistant communication systems. Their adaptability across diverse bands and future-proof potential make them suitable for 5G, 6G, IoT, and biomedical applications. The reference [27], A Historical Development and Futuristic Trends of Microstrip Antennas, gives a thorough examination of the history, design, and performance advances of microstrip patch antennas. It finds that using appropriate substrate materials, such as FR4 and conductive elements, such as copper or gold, increases antenna stability and performance. According to the study, modern geometrical configurations such as hexagonal, elliptical, T-stub, U-slot, and fractal structures improve bandwidth, impedance matching, and radiation efficiency by up to 180% and 95%, respectively, when compared to conventional rectangular patches. Among several feeding strategies, proximity and aperture coupling have been shown to be the most successful in terms of broad bandwidth and polarization purity. The report also underlines the increasing relevance of reconfigurable and multi-band antenna designs that use electrical, optical, and mechanical switching techniques to satisfy the needs of new technologies like as 5G, MIMO, and biomedical telemetry systems.

Overall, the study finds that MPAs may provide high gain, wide bandwidth, and compactness via optimal shape, material selection, and manufacturing procedures, making them crucial for next-generation wireless and satellite communication applications. In [28] is presented a compact ultra-wideband (UWB) antenna designed for millimeter-wave (mm-wave) and sub-6 GHz (FR2) 5G applications. Using a patch size enhancement technique without changing the substrate dimensions, the design achieves excellent impedance matching, low loss, and dual resonances at 32.5 GHz and 48.14 GHz with peak gains of 5.43 dBi and 10.86 dBi, respectively. The antenna, fabricated on a Rogers RT Duroid 5880 substrate, demonstrates a broad operating band from 26–60 GHz, linear polarization, and stable radiation patterns suitable for aeronautical, radar, and satellite systems. The study also validates an RLC equivalent circuit and shows that the proposed patch enhancement method can significantly boost gain and bandwidth for future 5G, Ka-, U-, and V-band applications while maintaining compactness and low fabrication cost. In [29] is present a novel design of a low-cost microstrip antenna intended for millimeter-wave (mm-wave) applications, primarily focusing on improving the depth of the reflection coefficient ($S_{11}$) below -20 dB, which is crucial for efficient power delivery and minimal signal loss in high-frequency communication systems. The authors achieve this enhancement by etching an open polygon slot at the lower edge of the antenna's patch and optimizing the ground plane, resulting in significantly improved impedance matching, a wide bandwidth of 6 GHz (34.72–40.72 GHz), and multiple gain peaks exceeding 10 dBi. Compared to earlier state-of-the-art designs that relied on more expensive substrates, the proposed antenna uses FR4 material, offering substantial cost savings and ease of fabrication without compromising performance, and demonstrating suitability for next-generation mm-wave practical implementations. The reference [30] describes a new Asymmetric Irregular Hexagonal Fractal (AIHF) millimeter-wave antenna with a low-loss substrate, a unique fractal-slot patch, and an Asymmetric Defected Ground Structure (ADGS) that is optimized for high gain and broad bandwidth. This antenna provides over 5.0 dBi gain across a −10 dB $S_{11}$ bandwidth of 4.655 GHz (32.84-37.215 GHz), with a peak gain of 13.4 dBi and an exceptional average radiation efficiency of 87.75%. Simulation and experimental validation reveal that the carefully constructed patch and ground asymmetries are fundamental to its improved performance, making the design attractive for advanced mm-wave applications. This research, [31], presents a low-cost, wide-band millimeter-wave prototype antenna designed on an FR4 substrate featuring a Defected Ground Structure (DGS) with concentric circles and dumbbell-etched slots for improved gain and bandwidth. The antenna achieves a −10 dB bandwidth of 3.89 GHz (30.26–34.15 GHz) with over 99% power efficiency and multiple gain peaks up to 9.83 dBi, making it suitable for 5G and futuristic network and robotic control applications. The design is validated experimentally via Vector Network Analyzer and anechoic chamber measurements, and an equivalent circuit model is also developed for performance analysis.

### *A. Motivation of Research*

Designing an efficient feeding network for antenna arrays remains a significant challenge, especially when aiming for high gain, wide bandwidth, and stable impedance matching. Conventional contact-based feeding techniques frequently suffer from signal losses at the physical interface, leading to mismatched impedance and reduced system efficiency. This drawback has led to a surge of interest in non-contact or

mutually coupled feeding techniques, which mitigate contact-related losses and enhance overall antenna performance.

Fractal geometries and specifically Cantor-set based slots produce self-similar multiband behaviour and size reduction that are attractive for C-band and satellite links, enabling wide impedance bandwidth and multiple resonances from a compact footprint [32]. Meanwhile, loading radiating elements with metamaterial inclusions such as split-ring resonators (SRRs) has been shown to improve miniaturization, create additional resonances and improve bandwidth or radiation performance when carefully integrated with fractal geometries [33-35]. However, when radiating elements are packed into arrays to achieve the gain and directivity required for satellite applications, mutual coupling between elements becomes a performance-limiting factor increasing correlation, distorting beam patterns, and degrading realized gain and efficiency. Effective array feeding and decoupling strategies are therefore essential. Recent studies both review mutual-coupling reduction techniques (DGS, EBG, metasurfaces, neutralization lines, etc.) and show that tailored feed/network approaches can control or even exploit coupling to produce compact, high-efficiency arrays [36-37].

Combining Cantor fractal slots with SRR loading and a mutually-coupled feeding technique aims to deliver a compact array that (a) achieves the multiband/miniaturization advantages of fractals, (b) benefits from SRR-based metamaterial enhancements, and (c) uses an informed feed/decoupling approach to preserve isolation, radiation efficiency and beam quality making it well suited for modern satellite C-band terminals and small satellite payloads.

### *B. Research Objectives*

This research aims to address critical knowledge gaps in the design and performance optimization of microstrip antenna arrays by focusing on the following objectives:

The primary objective of this work is to develop a novel non-contact (mutually coupled) feeding technique that effectively mitigates the fringing effect and enhances impedance matching, thereby improving the gain and bandwidth of the antenna array. In contrast to conventional contact-fed systems, this approach offers reduced losses and simplified integration, making it suitable for high-performance wireless systems.

Another significant objective is the miniaturization of the antenna structure through the use of a fractal slotted geometry, specifically employing two oppositely placed Cantor fractal units. This configuration enables compactness without compromising the antenna's radiation characteristics or bandwidth.

Furthermore, the study introduces a novel slot antenna design that demonstrates ultra-wideband behavior by combining fractal geometry with a mutually coupled feed mechanism. To further enhance performance, a split ring resonator (SRR) is incorporated into the ground plane to investigate its influence on gain and bandwidth characteristics.

The proposed antenna is uniplanar, low-cost, and easy to fabricate, utilizing an FR-4 substrate, and is well-suited for integration with Monolithic Microwave Integrated Circuits (MMICs). Given its performance benefits and design versatility, the antenna is highly applicable to a broad spectrum of modern communication systems, including satellite communications, radar systems, mobile MIMO platforms, 6G wireless networks, the Internet of Things (IoT), and WLANs.

The paper is organized as follows. Section 2 describes the material and method. Section 3 gives an overview of the studied parameters. Simulated and measured results are presented and discussed in Section 4. Finally, conclusions are presented in Section 5.

## II. MATERIALS AND METHODS

### *A. Feeding Network Design*

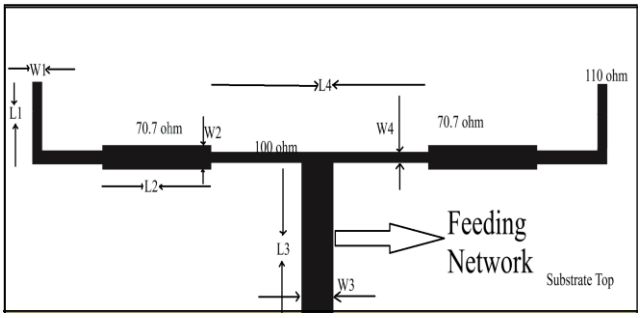


Fig.1. Feeding network

TABLE 1
FEEDING NETWORK DESIGN VARIABLES

| Variable | Dimension (mm) |
|---|---|
| Length of fed line (110 ohm) L1 | 11.76 |
| Width of fed line (110 ohm) W1 | 0.9 |
| Length of fed line (70.7 ohm) L2 | 10.52 |
| Width of fed line (70.7 ohm) W2 | 1.62 |
| Length of fed line (50 ohm) L3 | 10.27 |
| Width of fed line (50 ohm) W3 | 3.05 |
| Length of fed line (100 ohm) L4 | 21.56 |
| Width of fed line (100 ohm) W4 | 0.7 |

### *C. Process of Proposed Antenna Design with Resultant Fractal Curve*

A small-sized (37.33 mm × 87.2 mm x 1.6 mm) resultant fractal slotted (as depicted in Fig. 2) ultra-wideband (UWB) antenna is constructed on a thin 1.6 mm FR-4 substrate with a relative permittivity of 4.4 and a loss tangent (tan $\delta$ =0.02). The FR-4 substrate is commonly utilized for frequencies below 12 GHz [38]. Low-cost substrate antenna designs can be used at frequencies below 12 GHz. The suggested antenna design was analyzed and computed using an ANSYS Electronic Desktop Terminal (EDT), namely HFSS. The antenna under consideration has been specifically engineered to operate at a frequency of 7.8 GHz. A feeding network (as depicted in Fig.1) was employed to achieve perfect impedance matching with a 50 Ω center-fed transmission line. This feeding network is not directly connected with the patch but is mutually coupled with the patch to avoid contact losses and

perfect impedance matching. To avoid the fringing effect at the corner perfect dimension of the patch cut was obtained by using a parametric approach (as depicted in Table 3). Next, a cantor and an inverted cantor curve are presented. Afterward, the ideal length of the ground was found using the optimization tool of HFSS, resulting in an optimized length of 10.63 mm for DGS. Finally, a split ring resonator is introduced at ground to further improve in total gain and bandwidth. This allows us to attain a double-wideband bandwidth, namely ranging from 7.05 to 8.53 GHz and 10.2 to 11.5 GHz.

*C. Antenna Design*

Figure 2 (a), Tables 2 and 3 represent the variable's values.

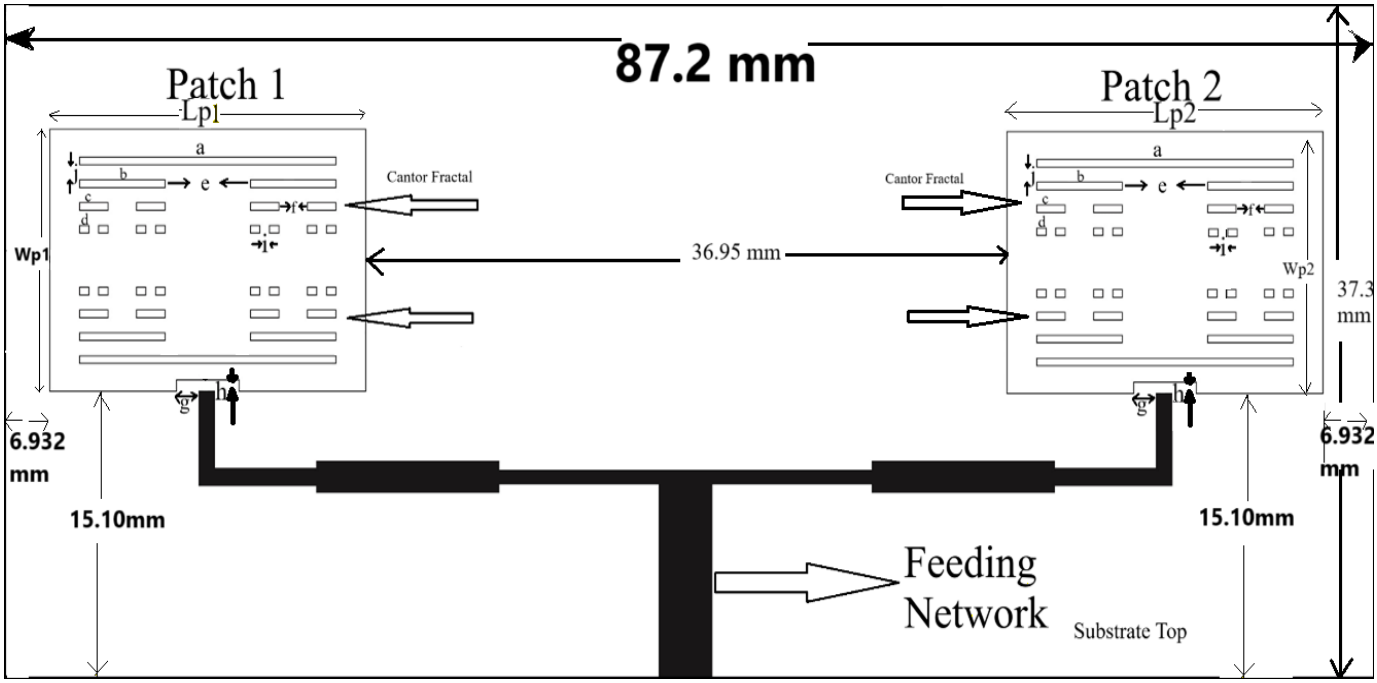


(a)

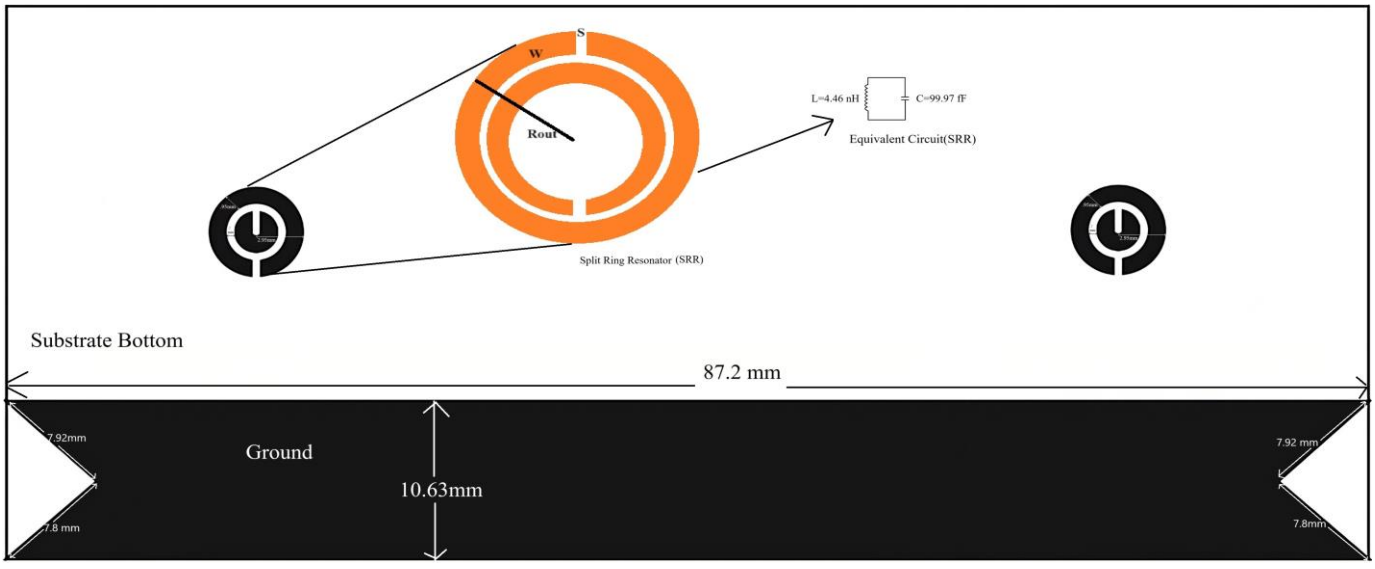


(b)

Fig.2. (a) Top view (b) Bottom view

TABLE 2
PROPOSED ANTENNA VARIABLES

| Variable | Dimension (mm) |
|---|---|
| Width of Patch 1(Wp1) and Patch 2 (Wp2) | 13.76 |
| Length of Patch1(Lp1) and Patch 2(Lp2) | 18.25 |
| A | 14.8 |
| B | 4.93 |
| C | 1.64 |
| D | 0.54 |
| E | 4.93 |
| F | 1.64 |
| I | 0.54 |
| Rout | 2.95 |
| W | 0.95 |
| S | 0.7 |

*D. Antenna Fabrication*

The antenna, created along with optimum dimensions by photolithography, UV exposure, and chemical etching, is produced on a 1.6 mm thick flame-retardant-4 epoxy substrate shown in Fig. 3(a) and 3(b). The constructed antenna undergoes testing for $S_{11}$ validation using the Agilent N5247A VNA.

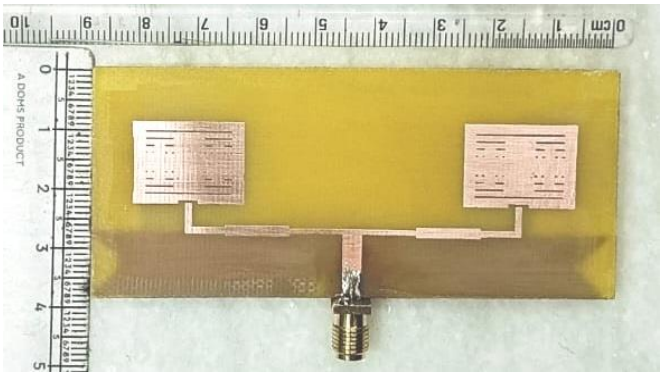

(a)

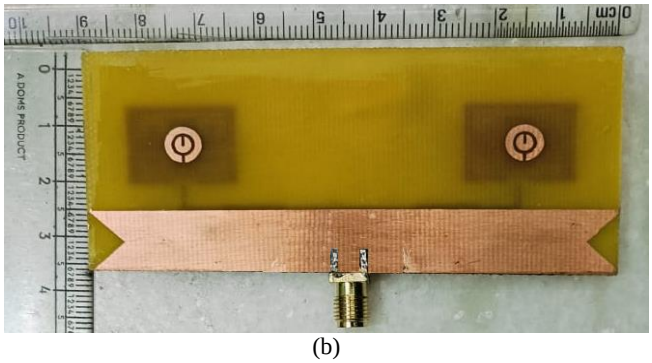

(b)

Fig. 3. (a) Fabricated (top), (b) Fabricated (bottom)

## III. MATHEMATICAL CALCULATIONS

The following parameters are used for the proposed antenna design.

| | |
|---|---|
| Dielectric Constant | 4.4mm |
| Dielectric Height(h) | 1.6mm |
| Frequency | 7.8 GHz |
| Permittivity ($\varepsilon_r$) | 2.2 for FR-4 |

*A. Fringing Effect*

The fringing effect in antennas denotes the occurrence wherein the electromagnetic field lines at the antenna's edges or corners bend and curve, resulting in a non-uniform radiation pattern. The fringing effect may result in a distorted radiation pattern, increased sidelobes, and diminished antenna efficiency. To mitigate the fringing effect, smoothing antenna edges, employing corner reflectors, and optimizing antenna design can be utilized [40]. In this study, the authors employ a novel optimized antenna design to mitigate the fringing effect at the junction of the fed and patch through a parametric approach. Table 3 shows that the optimized value of g and h at the resonance frequency 7.8 GHz is 1.3 mm and 0.6 mm, respectively.

TABLE 3
OPTIMIZING THE ANTENNA PARAMETERS

| S.No | Parameter g (mm) | Parameter h (mm)taken constant | Value of $S_{11}$ in dB | Frequency (GHz) |
|---|---|---|---|---|
| 1 | 0.4 | 0.6 | -34.5 | 7.8 |
| 2 | 0.7 | 0.6 | -36.7 | 7.8 |
| 3 | 1 | 0.6 | -38.2 | 7.8 |
| 4 | 1.3 | 0.6 | -42.34 | 7.8 |
| 5 | 1.6 | 0.6 | -28.2 | 7.8 |
| 6 | 1.7 | 0.6 | -26.3 | 7.8 |

| S.No | Parameter g (mm)taken constant | Parameter h (mm) | Value of $S_{11}$ in dB | Frequency (GHz) |
|---|---|---|---|---|
| 1 | 1.3 | 0.3 | -38.4 | 7 |
| 2 | 1.3 | 0.6 | -42.34 | 7.8 |
| 3 | 1.3 | 0.9 | -37.2 | 7.8 |
| 4 | 1.3 | 1.2 | -30.3 | 7.9 |
| 5 | 1.3 | 1.5 | -28.2 | 8 |
| 6 | 1.3 | 1.7 | -27.5 | 8 |

*B. Mutual Coupling Effect*

Mutual coupling denotes the interaction of two or more antennas or antenna elements, wherein the radiation pattern, impedance, and other attributes of one antenna are influenced by the presence of another antenna.

A minimum separation of 0.5λ (half a wavelength) between patches is advised to reduce mutual coupling [41]. For more rigorous specifications, a separation of 1λ (one wavelength) or greater may be required. The minimum distance for other types of patch antennas, such as slot-loaded and aperture-coupled, may vary based on the specific design and frequency range.

Figure 2 (a) shows the distance between the patches is 36.95 mm, which is greater than 0.5λ.

$$0.5\lambda = 0.5\left(\frac{c}{f}\right) = 19.73mm \quad (1)$$

## IV. Outcomes and Conversations

### A. Reflection Coefficient Vs Frequency

Reflection coefficient is a measure of how much power is reflected at an interface between two transmission lines or media, rather than being transmitted forward. A reflection coefficient of -10 dB or lower indicates that only a small fraction of the power is reflected, while the majority is transmitted. Specifically, a reflection coefficient of -10 dB corresponds to about 10% of power being reflected and 90% transmitted [42].

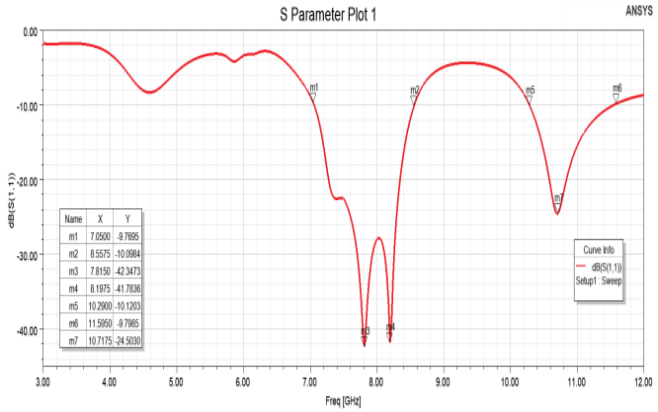


(a)

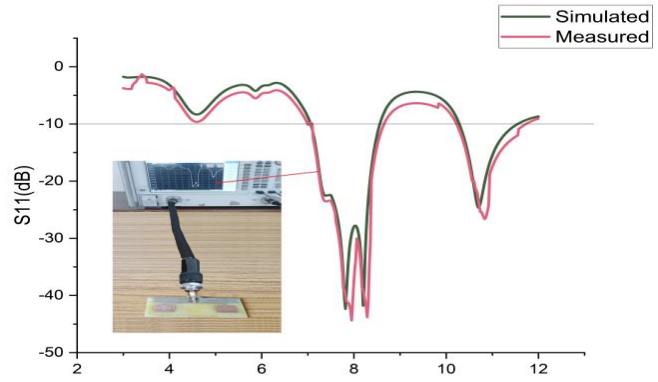


(b)

Fig. 4. (a) $S_{11}$ Plot (Simulation done on 7.8 GHz Frequency using HFSS), (b) Comparison between Simulated and Measured results (plotted in Origin software)

According to Figs. 4(a) and 4(b), it is pretty obvious that the values that were simulated and those that were measured are slightly different. This is because of the soldering effect that occurs during the fabrication process.

### B. Gain Plot

In the context of antennas, a gain plot represents the directional dependence of an antenna's gain. It's a graphical representation of how the antenna's gain varies in different directions. A gain plot for an antenna typically shows the gain (in decibels, dB) as a function of azimuth angle (θ) and elevation angle (φ).

The gain plot is illustrated in Fig. 5(a), 5(b), and 5(c) depict the simulated gain response of the proposed antenna across the operating frequency spectrum. As observed, the antenna demonstrates multiple resonant peaks with notable variations in gain corresponding to different frequency bands. At 7.8 GHz, as shown in Fig. 5(a), the antenna achieves a maximum gain of 7.9 dB, indicating strong radiation performance and efficient power transfer in this frequency band. This high gain is particularly advantageous for applications requiring long-range and directional communication, such as radar or satellite links in the X-band.

In Fig. 5(b), the gain at 8.1 GHz reaches 5.8 dB, which, while slightly lower than the previous peak, still represents a robust gain level suitable for medium-to-high data rate transmission in short- to medium-range communication systems.

Further, Fig. 5(c) illustrates a gain of 5.58 dB at 10.7 GHz, showing the antenna's capability to maintain good radiation performance at higher frequencies. This gain value confirms the antenna's effective operation in the upper end of the UWB spectrum, making it suitable for high-frequency applications such as advanced imaging systems and high-resolution sensing.

Overall, the gain profile reveals the antenna's ability to maintain consistently strong performance across multiple resonant frequencies, thereby validating its suitability for multiband UWB applications with minimal performance degradation at higher frequencies.

### C. Field Plot

The E plot facilitates the visualization of the antenna's emission pattern, illustrating the direction and intensity of the electric field. These plots also explain the intensity of the electric field at various locations surrounding the antenna. The J plot illustrates the current distribution on the antenna, aiding engineers in comprehending the excitation of the antenna. The J plot can also reveal regions of elevated current density, potentially resulting in heightened losses and diminished antenna efficiency. Here Fig. 6(a), 6(b), 6(c), 6(d), 6(e) and 6(f) shows the E-field and J-field plot at resonance frequencies.

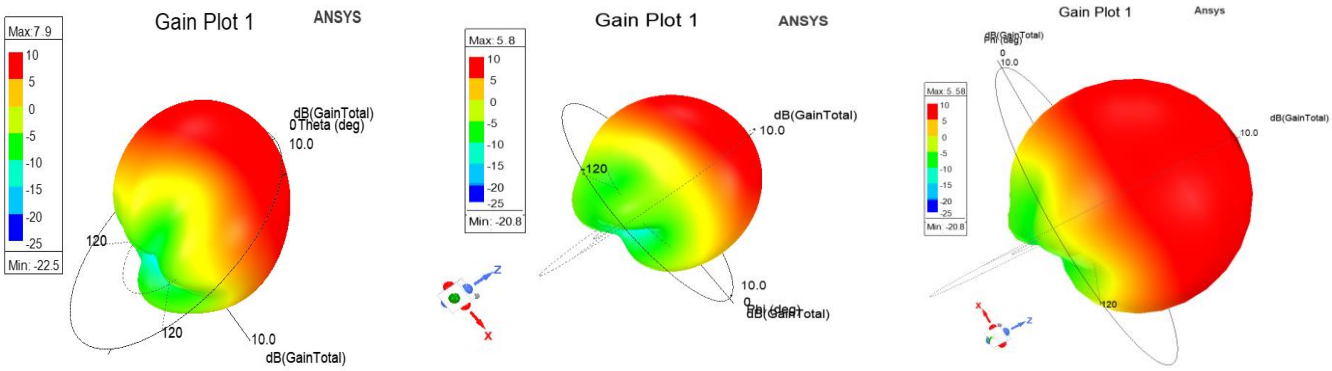


(a) (b) (c)

Fig. 5. (a) Gain at 7.8 GHz, (b) Gain at 8.1 GHz, (c) Gain at 10.7 GHz

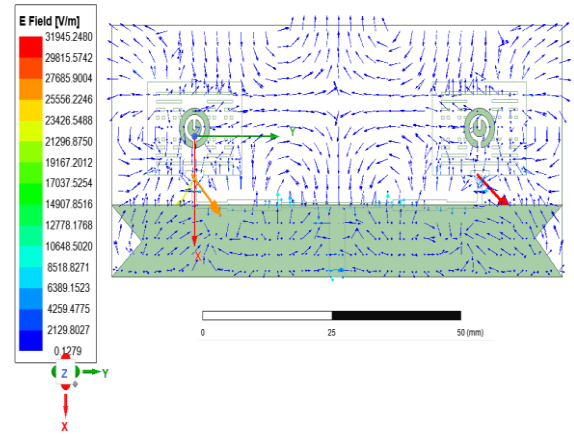


(a)

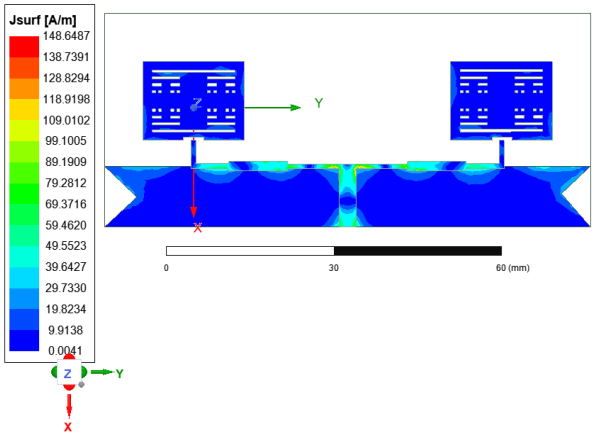


(b)

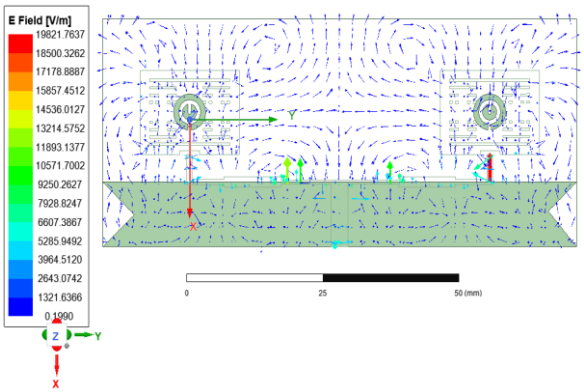


(c)

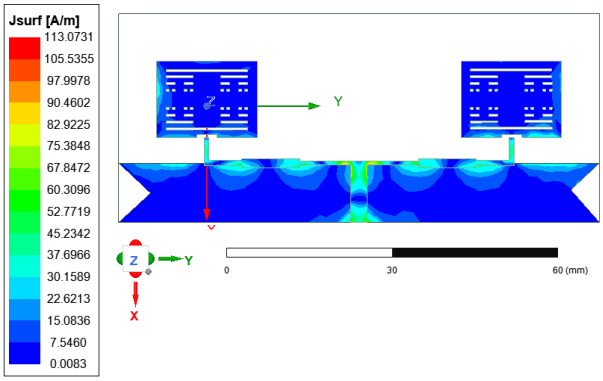


(d)

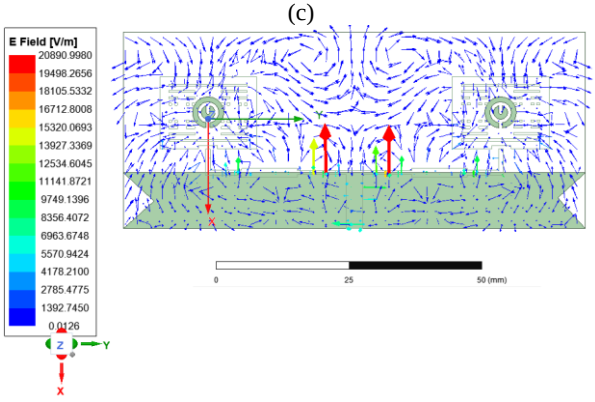


(e)

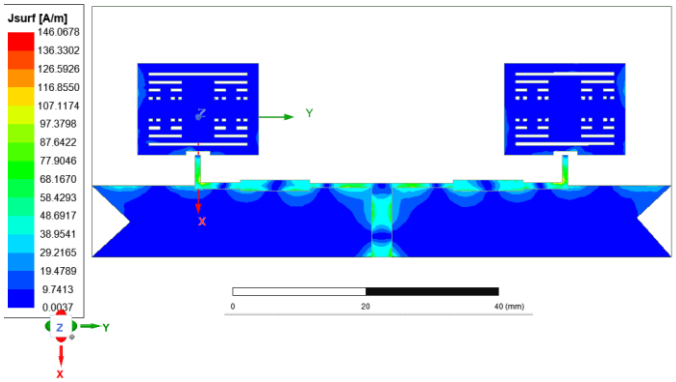


(f)

Fig. 6. (a) E-field(V/m) at 7.8 GHz, (b) J-field(A/m) at 7.8 GHz, (c) E-field(V/m) at 8.1 GHz, (d) J-field(A/m) at 8.1 GHz, (e) E-field(V/m) at 10.7 GHz, (f) J-field(A/m) at 10.7 GHz

*D. Gain Vs Frequency Plot*

The gain vs frequency plot is a graphical representation of an antenna's gain (directivity) as a function of frequency. This plot provides valuable insights into an antenna's performance across different frequencies. The y-axis represents the antenna's gain, typically measured in decibels relative to isotropic (dBi). The x-axis represents the frequency range over which the antenna's gain is measured. The frequency at which the antenna's gain is maximum is called the resonance frequency. The plot helps determine if the antenna is tuned to the desired frequency. A peak in the gain at the desired frequency indicates proper tuning. The plot reveals the antenna's bandwidth, which is essential for applications requiring operation over a range of frequencies. The gain vs frequency plot can also provide insights into the antenna's efficiency, as a higher gain typically indicates higher efficiency. Here in Fig. 7, the gain remains almost constant between 7.05-8.53 GHz and 10.2–11.5 GHz. Peak gain is obtained at frequencies 7.8 GHz and 10.7 GHz.

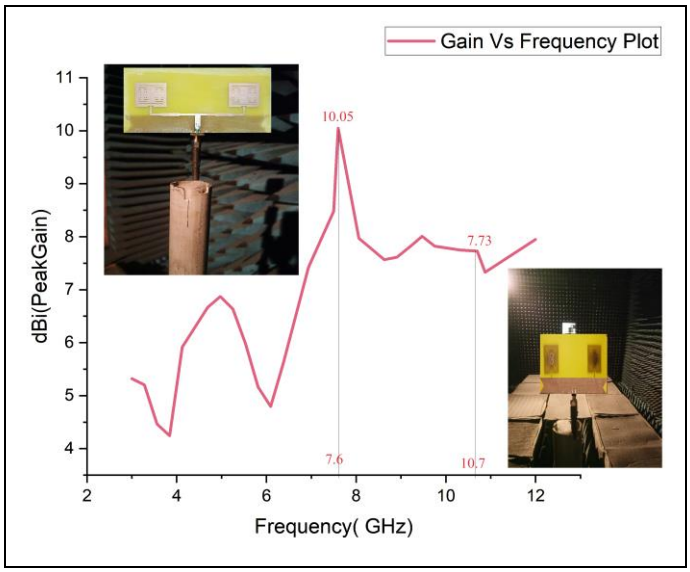


Fig. 7. Gain Vs Frequency Plot

*E. Radiation Pattern Plot*

A radiation pattern plot is a graphical representation of an antenna's radiation properties, showing how the antenna radiates energy in different directions. It's a crucial tool for understanding an antenna's performance and behaviour. The E-plane is defined as the plane that contains the electric field vector (E) and the direction of maximum radiation. For a linearly polarized antenna, the E-plane is typically aligned with the antenna's electric field vector. When Phi=90, the E-plane is aligned with the x-axis (or the horizontal plane), which means the electric field vector is parallel to the x-axis [22]. The H-plane is defined as the plane that contains the magnetic field vector (H) and is perpendicular to the E-plane. For a linearly polarized antenna, the H-plane is typically aligned with the antenna's magnetic field vector. When Phi=0, the H-plane is aligned with the y-axis (or the vertical plane), which means the magnetic field vector is parallel to the y-axis [22]. The simulated and measured radiation plot in E-plane and H-plane is displayed in Figs. 8(a), 8(b), 8(c), 8(d), 8(e), and 8(f). All simulation is carried out in HFSS, and a comparison plot between the simulated and measured values is plotted in origin software.

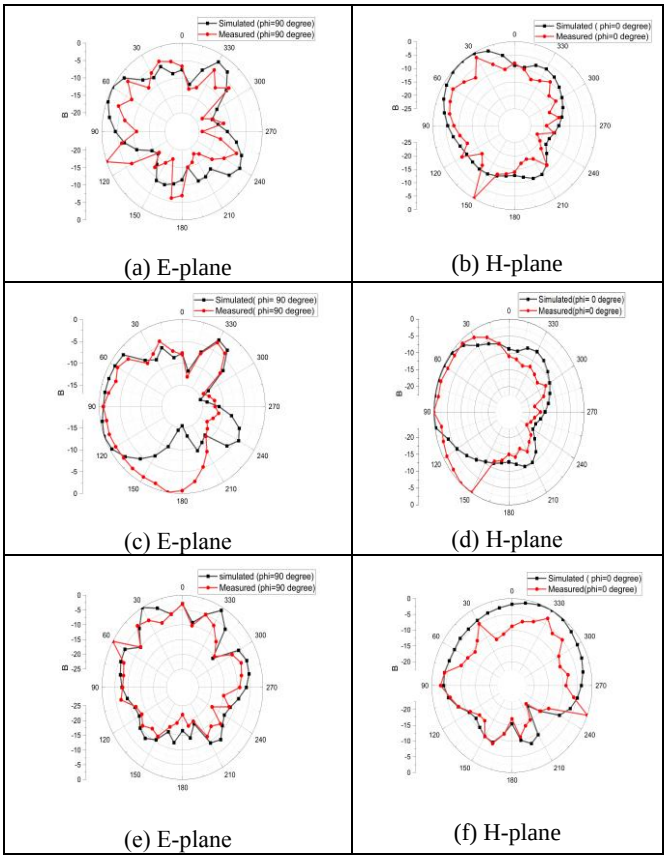


Fig. 8. (a) Radiation pattern at 7.8 GHz (E-plane), (b) Radiation pattern at 8.1 GHz(H-plane), (c) Radiation pattern at 8.1 GHz (E-plane), (d) Radiation pattern at 8.1 GHz(H-plane), (e) Radiation pattern at 10.7 GHz (E-plane), (f) Radiation pattern at 10.7 GHz (H-plane)

TABLE 4
SIMULATED AND MEASURED RESULTS OF THE PROPOSED ANTENNA

| Antenna | Res. Freq., fr(GHz) | Ref. Coeff icient , S11[dB] | BW (GHz) | FBW (%) | Gain (dBi) |
|---|---|---|---|---|---|
| Simulated | 7.8/8.1/ 10.7 GHz | -42.34/ -41.7/ -24.5 | 7.05-8.53 GHz/ 10.33–11.43 GHz | 18.9/ 12.1 | 10.0 5/7.7 3 |
| Measured | 7.9/8.15/ 10.75 | -44.3/ -43.2/ -25.2 | 7.05- 8.61GHz/10.33- 11.54 GHz | 19.7/ 11.5 | 10.0 5/7.7 3 |

Table 4 presents the simulated and measured outcomes of the proposed antenna. The table indicates that the simulated and measured results are quite comparable.

TABLE 5
PERFORMANCE COMPARISON OF THE PROPOSED ANTENNA WITH THE EXISTING LITERATURE

| Ref. | Year | Substrate & feeding | Fractal / Slot Type | Size (mm²) | Res. Freq. (GHz) | −10 dB BW (GHz) | FBW (%) | Peak Gain (dBi) | Highlights |
|---|---|---|---|---|---|---|---|---|---|
| [45] | 2015 | Rogers RO4003, Proximity-fed | 9-Square Log-Periodic Fractal | 173×70 | 3.2–10.9 | 3.1–11.0 | Up to 45.81 | ~11.15 @ 5 GHz | Wideband; large size |
| [10] | 2019 | RT Duroid 5880, Inset-fed | Double T-shaped Slots | 20×16.5 | 10 / 28 / 38 | 9–39 | 20 / 7.14 / 5.26 | ~11.72 @ 38 GHz | High gain; mmWave applications |
| [11] | 2013 | Coaxial-fed | Double U-slots | 50×50 | 3.6 / 5.2 | 3.49–5.42 | 7.5–9.6 | ~8.5–8.6 | Dual-band simple geometry |
| [12] | 2017 | FR-4, Inset-fed | 5 Rectangular + 5 Circular Slots | 55×35.5 | 2.81–8.72 | Multiband ranges | ~5–12 | Up to ~11.45 | Moderate FBW, slot diversity |
| [14] | 2021 | RT Duroid 5880, Edge-fed | Ear-shaped Circular Slot | 40×45 | 7.4–38.6 | 1.22–47.5 | ~190 | Varies 0.2–9.7 | Very wide FBW; variable gain |
| [44] | 2021 | FR-4, Edge-fed | Tri-Rectangular Fractal Arms | 66.4×66.4 | 2.45 | 1.81–3.0 | ~49 | ~7.16 | Good bandwidth; simple layout |
| [39] | 2019 | FR-4, Inset-fed | Dual Koch-slot Fractal | 37.29×29.06 | 2.4–9.4 | 2.3–9.7 | ~6–10 | ~5.71 @ 2.37 GHz | Compact UWB with moderate gain |
| [43] | 2018 | FR-4, Transformer-fed | Koch–Koch / Koch–Minkowski Hybrid | 45×38.92 | 2.46–8.38 | 2.38–10.0 | ~8–29 | ~5.73 / 5.62 | Hybrid fractal shapes with moderate gain |
| [46] | 2023 | FR-4, Offset Edge-fed | Koch–Minkowski Hybrid Fractal | 38.12×38.42 | 3.2–10.10 | 2.85–11.32 | ~119.6 | ~8.26 | Wide multiband coverage |
| [47] | 2024 | Coaxial-fed | Circular-ring shaped fractal (central "+" + 8 small rings) | 38×45 | 1.75 | 2.05–14.5 (UWB: 3.1–10.6) | 95 | 2–6.5 | PSO-optimized compact UWB fractal on Rogers RT5880 |
| [48] | 2024 | FR-4 ($\varepsilon_r$ = 4.4, h = 1.6 mm); microstrip 50 Ω feed | Sierpinski hexagonal-shaped fractal (partial ground with 3 stubs & 3 slits) | 24 × 30 | 2.41; 6.59; 9.80 | 2.19–4.43 ; 4.8–7.76 ; 8.04–11.32 (bandwidths 2.24 ; 2.96 ; 3.28 GHz) | 67.7 % 47.1 % 33.9 % | 1.07 at ~2.5 GHz 4.19 at ~6.6 GHz 4.01 at ~9.8 GHz | Compact Size With Tri-Wideband Operation, Modified Partial Ground Plane, Covers Many Practical Wireless Bands |
| [49] | 2024 | FR-4, SIW + DGS | Sierpinski + SIW-Based mmWave Fractal | Compact | 25.8–37.7 | up to ~11.4 | High | ~5.9 | mmWave UWB in compact SIW + Sierpinski setup |
| [50] | 2023 | FR-4 (CPW-fed) | Circular Cantor Hybrid | 40 × 50 | 3.1 / 5.8 / 9.6 | 2.9–10.1 | 9.89–16.12 | 6.84–7.12 | Efficient compact CPW fractal for multiband comm. |
| [51] | 2023 | FR4 (εr = 4.3, h = 1.66 mm) + TMM4 (for comparison) Feed: Coax + 1×2 Wilkinson Power Divider Network | Combined Minkowski–Sierpinski fractal 2×2 | ~38.5 × 25 mm Array: 240 × 240 mm (with aluminum ground) | 4.17 / 5.97 | 0.085 / 0.182 | 2.03-3.05 | 4.19-9.6 | Novel Hybrid Fractal Geometry, Dual-Band Operation for Modern Wireless Standards, High-Gain 2×2 Antenna Array, Wideband & Efficient Wilkinson Power Divider Feeding Network |
| [52] | 2020 | FR-4 (standard PCB material) + microstrip feed | Complementary Sierpinski gasket fractal patch + complementary Archimedean Defected Ground Structure (DGS) | compact design for portable 4G/5G UWB MIMO) | UWB covering wideband frequencies (exact resonant frequency not a single value) | 3.2–8.6 | 8.53–17.14 | 6.23–7.1 | DGS-enhanced UWB with good isolation |
| [53] | 2023 | FR-4 ($\varepsilon_r$ = 4.4, tanδ ≈ 0.02), 50 Ω microstrip feed | Circular-resonator with square slots + fractal-like slotting + partial-ground-plane | 40 × 34 | Dual wide-band: ~2.30–4.10 and ~6.10–10.0; resonances at 2.8, 3.51, 6.53, 9.37 GHz | ~1.80 GHz (2.30–4.10); ~3.90 GHz (6.10–10.0) | ~56% ~48% | 2- 9 | Compact & Low-Cost Substrate, Dual-Wideband (effectively UWB coverage), High Gain & High Efficiency, Simple Geometry: Circular Patch + Square-Slot Fractal + Partial Ground + Gap Line |
| [54] | 2024 | FR-4 (CPW-fed) | Modified Sierpinski square | 34 × 34 | 3.8 / 5.2 / 9.1 | 3.1–10.6 | 119.55 | 3.8 / 3.6 / 2.9 | UWB with 5.2 GHz band notch filtering |
| **This Work** | **2025** | **FR-4, Novel Mutual-Coupled Fed** | **Cantor + Inverted Cantor + DGS** | **37.33×87.2** | **7.8 / 10.7** | **7.05–11.5** | **18.9 / 12.1** | **10.05 @ 7.8 GHz / 7.95 @ 8.1 GHz / 7.73 @ 10.7 GHz** | **High-gain dual-band UWB; compact; novel fed design** |

Comparison Table 5 shows several fractal and slot-based antenna designs that were disclosed between 2013 and 2025. It shows their substrates, geometries, operating bands, and performance. Early efforts (e.g., [45], [11], [12]) mostly used substantial structures and simple slot configurations, resulting in limited bandwidth and gain. Over time, researchers moved toward smaller FR-4 and RT Duroid substrates that used hybrid fractal geometries like Koch, Minkowski, Sierpinski, and Cantor structures. These were often combined with Defected Ground Structures (DGS) or Substrate Integrated Waveguide (SIW) techniques to improve bandwidth and make things smaller. Recent designs (2023–2025) show amazing progress, with fractional bandwidths over 100% and gains of about 7–10 dBi. These designs are good for multiband, UWB, and 5G/mmWave applications. The suggested work (2025) using an innovative mutual-coupled Cantor–Inverted Cantor configuration on FR-4 exhibits exceptional dual-band UWB performance, achieving high gain (up to 10.05 dBi) and a small form factor, surpassing the efficiency and bandwidth compactness of most prior systems.

### *F. Application of Proposed Antenna*

The 7.8 GHz is utilized for satellite uplink and downlink communications, necessitating high-gain antennas for effective data transfer. This frequency is employed in radar systems for surveillance, navigation, and meteorological observation, requiring antennas with elevated directivity and resolution. 7.8 GHz belongs to the millimeter-wave frequency band, utilized for high-speed WLANs, necessitating antennas with elevated gain and beamforming capabilities. This frequency is under investigation for application in forthcoming cellular networks, necessitating antennas with elevated gain, beamforming, and extensive MIMO functionalities. 7.8 GHz is utilized in remote sensing applications, including soil moisture assessment and crop surveillance, necessitating antennas with high resolution and precision. This frequency is employed in military communications for secure and dependable data transfer, requiring antennas with high gain, beamforming capabilities, and a low probability of interception. X-band frequencies, including 8.1 GHz, are used for space exploration, such as deep space communications and navigation. 10.7 GHz is utilized for satellite television, telecommunications, and meteorological forecasting, necessitating high-gain antennas. 10.7 GHz is also utilized for the surveillance of soil moisture, agricultural health, and meteorological patterns.

## V. CONCLUSIONS

In this study, a novel mutual-coupled fed ultra-wideband (UWB) antenna array based on a Cantor fractal slotted design with a Defective Ground Surface (DGS) configuration has been successfully designed, fabricated, and experimentally evaluated. The proposed antenna is tailored for operation across both the C-band (4–8 GHz) and X-band (8–12 GHz) frequency ranges, making it highly versatile for a wide spectrum of modern wireless applications.

The antenna is implemented on a low-cost FR-4 substrate with compact dimensions of 37.33 mm × 87.2 mm × 1.6 mm, ensuring economic feasibility and practical manufacturability. The measured and simulated results exhibit a strong correlation in terms of return loss and radiation characteristics, with only minor discrepancies observed at the resonant frequencies. Within the measured UWB range of 7.05–8.53 GHz and 10.2–11.5 GHz, the antenna demonstrates effective radiation behavior. Notably, the antenna achieves high peak gain values of 10.05 dBi at 7.8 GHz, 7.95 dBi at 8.1 GHz, and 7.73 dBi at 10.7 GHz, which highlight its superior radiation efficiency and suitability for long-range and high-throughput wireless systems. The mutual coupling-fed approach used in this design effectively reduces fringing fields and increases the electrical length of the radiator, resulting in improved impedance matching and more uniform radiation characteristics. A parametric optimization approach was employed to fine-tune the design parameters, minimizing the impact of parasitic effects and ensuring an undistorted radiation pattern across the targeted bands. Furthermore, Cantor and Inverted Cantor fractal geometries have been strategically integrated to achieve significant miniaturization without compromising electromagnetic performance, thus fulfilling the compactness requirements of modern RF front-ends. With an observed fractional UWB bandwidth of approximately 18.9%, the proposed antenna proves to be highly suitable for a wide range of contemporary and emerging communication systems, including but not limited to satellite communication, radar systems, WLAN, remote sensing, earth observation, and defense communication infrastructures.

Moreover, due to its efficient design and inherent scalability, the proposed antenna holds potential applicability in advanced domains such as Quantum Key Distribution (QKD) and Quantum Sensing. With further enhancements - particularly through the integration of Metamaterials and Frequency Selective Surfaces (FSS) - the gain and bandwidth performance can be elevated further, extending its viability into next-generation and secure communication platforms.

## ACKNOWLEDGMENT

The Measurements were conducted at the ECE Dept. Indian Institute of Technology (IIT), Roorkee. This provided access to the necessary equipment and resources.

## REFERENCES

[1] R. Azim and M. T. Islam, “Compact Planar UWB Antenna with Band Notch Characteristics for WLAN and DSRC,” in *Progress in Electromagnetics Research,* vol. 133, pp. 391–406, 2013, DOI: 10.2528/PIER12090601

[2] A. Syed and R. W. Aldhaheri, “A Very Compact and Low Profile UWB Planar Antenna with WLAN Band Rejection,” in *Scientific World Journal*, vol. 7, pp. 1–7, 2016, DOI: 10.1155/2016/3560938

[3] J. P. Gianvittorio and Y. R. Samii, “Fractal Antennas: a Novel Antenna Miniaturization Technique, and Applications,” in *IEEE Antennas and Propagation Magazine*, vol. 44, no. 1, pp. 20–36, 2002, DOI: 10.1109/74.997888

[4] Y.-L. Zhao, Y.-C. Jiao, G. Zhao, L. Zhang, Y. Song, and Z.-B. Wong, “Compact Planar Monopole UWB Antenna with Band-Notched Characteristic,” in *Microwave and Optical Technology*

*Letter*, vol. 50, no. 10, pp. 2656–2658, 2008, DOI: 10.1002/mop.23717

[5] H.-W. Liu, C.-H. Ku, T.-S. Wang, and C.-F. Yang, "Compact Monopole Antenna with Band-Notched Characteristic for UWB Applications," in *IEEE Antennas and Wireless Propagation Letters*, vol. 9, no. 1, pp. 397–400, 2010, DOI: 10.1109/LAWP.2010.2049633

[6] S. Patil and V. Rohokale, "Multiband Smart Fractal Antenna Design for Converged 5G Wireless Networks," *2015 International Conference on Pervasive Computing (ICPC)*, Pune, India, 2015, pp. 1-5, DOI: 10.1109/PERVASIVE.2015.7087020

[7] M. A. Abdalla, A. A. Ibrahim, and A. Boutejdar, "Resonator Switching Techniques for Notched Ultra-Wideband Antenna in Wireless Applications," in *IET Microwaves, Antennas & Propagation*, vol. 9, no. 13, pp. 1468-1477, 2015, DOI: 10.1049/iet-map.2014.0838

[8] F. B. Zarrabia, Z. Mansourib, N. P. Gandjic, and H. Kuhestanib, "Triple-Notch UWB Monopole Antenna with Fractal Koch and T-Shaped Stub," in *AEU - International Journal of Electronics and Communications*, vol. 70, no. 1, pp. 64-69, 2016, DOI: 10.1016/j.aeue.2015.10.001

[9] B. P. A. Mahatmanto and C. Apriono, "Rectangular Configuration Microstrip Array Antenna for C-Band Ground Station," *27th International Conference on Telecommunications (ICT)*, Bali, Indonesia, 2020, pp. 1-5, DOI: 10.1109/ICT49546.2020.9239576

[10] A. Abdelaziz, K. Ehab, and I. Hamad, "Design of a Compact High-Gain Microstrip Patch Antenna for Tri-Band 5G Wireless Communication," in *Frequenz*, vol. 73, pp. 45-52, 2018, DOI: 10.1515/freq-2018-0058.

[11] S. Liu, S. Qi, W. Wu, and D.-G. Fang, "Single-Fed Dual-Band Dual-Polarized U-Slot Patch Antenna," *IEEE MTT-S International Microwave Workshop Series on RF and Wireless Technologies for Biomedical and Healthcare Applications (IMWS-BIO)*, 2013, DOI: 10.1109/IMWS-BIO.2013.6756164

[12] N. Kaur and N. Sharma, "Designing of Slotted Microstrip Patch Antenna Using Inset Cut Line Feed for S, C, and X-Band Applications," in *International Journal of Electrical Engineering Research*, vol. 9, no. 7, pp. 957-969, 2017

[13] K. Shimizu and T. Fujimoto, "A Printed Inverted-F Antenna for Dual-Band Dual-Sense Circular Polarization," *IEEE International Workshop on Electromagnetics: Applications and Student Innovation Competition (iWEM)*, pp. 1-1, Aug. 2018, DOI: 10.1109/iWEM.2018.8536656

[14] A. Varshney, T. M. Neebha, V. Sharma, J. Grace, and A. Diana, "Dodecagon-Shaped Frequency Reconfigurable Antenna Practically Loaded With 3-Delta Structures for ISM Band and Wireless Applications," in *IETE Journal of Research*, pp. 1-13, 2022, DOI: 10.1080/03772063.2022.2034536

[15] A. K. Sharma, V. Sharma, and S. Singh, "Design and Performance Analysis of CSRR-Loaded High-Gain Multiband Rectangular Microstrip Patch Antenna Array (1x2) for IoT and Wireless Applications," *IEEE 3rd World Conference on Applied Intelligence and Computing (AIC)*, pp. 1185-1191, 2024, DOI: 10.1109/AIC61668.2024.10731106.

[16] A. K. Sharma, V. Sharma, and K. Kapoor, "Historical Development of Spatial Modulation and Massive MIMO Communication System with Implementation Challenges: A Review," in *International Journal of Sensors, Wireless Communications and Control*, vol. 11, no. 2, 2021, DOI: 10.2174/2210327910666200320093532

[17] A. Varshney, V. Sharma, and A. K. Sharma, "RLC-Equivalent Circuit Based Stub Loaded 2x2 MIMO Antenna for Wireless Applications," in *Microwave Review*, vol. 29, no. 1, 2023

[18] A. K. Sharma, V. Sharma, and S. Singh, "A Comprehensive Examination of the Current State of the Art in Fractal Array Antennas," in *Advances in Systems Science and Applications*, vol. 23, no. 4, 2023, DOI: 10.25728/assa.2023.23.04.1384.

[19] M. Marzouk et al., "Ultra-Wideband Compact Fractal Antenna for WiMAX, WLAN, C and X Band Applications," in *Sensors*, vol. 23, no. 9, p. 4254, 2023, DOI: 10.3390/s23094254

[20] P. Pannu, "Highly compact UWB-MIMO Antenna with Sharp Multi-Stop Band Characteristics," in *EURASIP Journal on Wireless Communications and Networking*, vol. 2024, no. 1, 2024, DOI: 10.1186/s13638-024-02369-1V

[21] V. Sukanya and S. N. Reddy, "UWB MIMO 4-Port Fractal Antenna with Reduced Mutual Coupling," in *IJRASET*, vol. 12, no. 4, 2024, DOI: 10.22214/ijraset.2024.61230

[22] N. Bisht, P. K. Malik, S. Das, T. Islam, S. Asha, M. Alathbah "Design of a Modified MIMO Antenna Based on Tweaked Spherical Fractal Geometry for 5G New Radio (NR) Band N258 (24.25–27.25 GHz) Applications," *Micromachines*, vol. 7, no. 10, p. 718, 2023, DOI: 10.3390/fractalfract7100718

[23] G. Dhandapani, S. Lavadya, S. Aldosary, W. El-Shafai, "Fractal-Shaped Super UWB (96THz) of Quadpot MIMO Antenna for 6G Communication," *Optical and Quantum Electronics*, vol. 56, no. 2, 2024, DOI: 10.1007/s11082-024-07416-1

[24] T. Kumari, A. N. Ghazali, A. Senapati, "Koch-Fractal Octagonal Antenna with DGS for UWB Usage," in *JJCIT*, vol. 13, no. 1, pp. 45–52, 2024, DOI: 10.5455/jjcit.71-1698995606

[25] A. Sohi et al., "UWB Aperture Coupled Circular Fractal Mimo Antenna with A Complementary Rectangular Spiral Defected Ground Structure (DGS) for 4G/ WLAN/ Radar/ Satellite/ International Space Station (Iss) Communication Systems," in *J. Electromagn. Waves Appl.*, vol. 34, no. 17, pp. 1934–1949, 2020, DOI: 10.1080/09205071.2020.1813638

[26] A. Bekasiewicz and M. Malek, "Ultra-Compact Spline-Optimized UWB Antenna Using Gradient-Based Metaheuristics," *arXiv preprint arXiv*:2503.13032, 2025

[27] S. Singh, G. Sethi, and J. S. Khinda, "A Historical Development and Futuristic Trends of Microstrip Antennas," in *International Journal of Computing and Digital Systems*, vol. 12, no. 1, 2022, DOI: 10.12785/ijcds/120117

[28] S. Singh, G. Sethi, and J. S. Khinda, "Low-Loss UWB mm-Wave Monopole Antenna Using Patch Size Enhancement for Next-Generation (5G and Beyond) Communications," in *Journal of Infrared, Millimeter, and Terahertz Waves*, 2023, DOI: 10.1007/s10762-023-00941-2

[29] S. Singh, G. Sethi, and J. S. Khinda, "Improvement in Depth of Reflection Coefficient Below -20 dB for Millimeter–Wave Antenna," in *Journal of Physics: Conference Series*, vol. 2327, no. 1, 2022, DOI: 10.1088/1742-6596/2327/1/012048

[30] S. Singh, G. Sethi, and J. S. Khinda, "Optimisation of Asymmetries in mm-Wave Single-Element Fractal Antenna for Gain-Bandwidth Enhancement," *International Journal of Electronics*, vol. 112, no. 5, pp. 795–816, 2025, DOI: 10.1080/00207217.2024.234080

[31] S. Singh, G. Sethi, and J. S. Khinda, "Improvement in Depth–of–Return–Loss and Augmentation of Gain-Bandwidth with Defected Ground Structure for Low-Cost Single-Element mm–Wave Antenna," in *International Journal of Computing and Digital Systems*, vol. 16, no. 1, pp. 101–113, 2024, DOI: 10.12785/ijcds/160108

[32] F. Ez-Zaki, H. Belahrach, and A. Ghammaz, "Broadband Microstrip Antennas with Cantor Set Fractal Slots for Vehicular Communications," *International Journal of Microwave and Wireless Technologies*, vol. 13, no. 3, pp. 1–10, 2020, DOI: 10.1017/S1759078720000719

[33] C. Elavarasi, T. Shanmuganantham, "SRR Loaded Periwinkle Flower Shaped Fractal Antenna for Multiband Applications,"

*Microwave and Optical Technology Letters*, vol. 59, no. 10, pp. 2518–2525, 2017, DOI: 10.1002/mop.30763

[34] N. Kaur, J. S. Sivia, M. Kumar, "SRR and Rectangular Stubs Loaded Novel Fractal Circular Antenna for Multiband Applications," *Wireless Personal Communication*, vol. 120, pp. 515-533, 2021, DOI: 10.1007/s11277-021-08472-6

[35] T. Shanmuganantham, S. A. Kumar, and D. Sindhahaiselvi, "CB-CPW fed SRR loaded ISM and 5G low profile antenna for on-body healthcare monitor," *Progress in Electromagnetic Research M*, vol. 109, pp. 25–38, 2022, DOI: 10.2528/PIERM22010701

[36] I. A. Tunio, Y. Mahe, T. Razban-Haghighi, and B. Froppier, "Mutual Coupling Reduction in Patch Antenna Array Using Combination of Shorting Pins and Metallic Walls," *Progress in Electromagnetic Research C*, vol. 107, pp. 157–171, 2021, DOI: 10.2528/PIERC20082803

[37] A. Kumar, A. Q. Ansari, B. K. Kanaujia, J. Kishor, and L. Matekovits, "A Review on Different Techniques of Mutual Coupling Reduction Between Elements of Any MIMO Antenna. Part 1: DGSs and Parasitic Structures," *Radio Science*, vol. 56, no. 3, pp. 1–16, 2021, DOI: 10.1029/2020RS007122

[38] N. Kaur and N. Sharma, "Designing of Slotted Microstrip Patch Antenna Using Inset Cut Line Feed for S, C and X-Band Applications," in *International Journal of Electronics Engineering Research*, vol. 9, no. 7, pp. 957-969, 2017

[39] D. Fonseca, F. Pereira, Ulysses, and R. C. Vitor, "Study of Patch Antennas with Koch Curve Form Slots," in *Journal of Microwaves, Optoelectronics and Electromagnetic Applications*, vol. 18, pp. 399-407, 2019, DOI: 10.1590/2179-10742019v18i31672

[40] W. L. Stutzman and G. A. Thiele, *Antenna Theory and Design*, John Wiley & Sons, 2012, ISBN: 978-0-470-57664-9

[41] C. A. Balanis, *Antenna Theory*, 2nd ed., New York, NY, USA: John Wiley & Sons, Inc., 1997

[42] D. M. Pozar, *Microwave Engineering*, 4th ed. John Wiley & Sons, Inc., 2012, pp. 26-30

[43] N. Sharma and V. Sharma, "A Design of Microstrip Patch Antenna Using Hybrid Fractal Slot for Wideband Applications," in *Ain Shams Engineering Journal*, vol. 9, pp. 249-2497, 2018, DOI: 10.1016/j.asej.2017.05.008

[44] A. Varshney, N. Cholake, and V. Sharma, "Low-Cost ELC-UWB Fan-Shaped Antenna Using Parasitic SRR Triplet for ISM Band and PCS Applications," in *International Journal of Electronics Letters*, vol. 10, no. 4, pp. 391-402, 2021, DOI: 10.1080/21681724.2021.1966655

[45] A. Amini and H. Oraizi, "Miniaturized UWB Log-Periodic Square Fractal Antenna," in *IEEE Antennas and Wireless Propagation Letters*, vol. 14, pp. 1322-1325, 2015, DOI: 10.1109/LAWP.2015.2411712

[46] S. Singh, A. Varshney, V. Sharma, I. Elfergani, C. Zebiri, and J. Rodriguez, "A Compact Off-Set Edge Fed Odd-Symmetric Hybrid Fractal Slotted Antenna for UWB and Space Applications," in *Progress in Electromagnetics Research B*, vol. 102, pp. 37–60, 2023, DOI: 10.2528/PIERB23052306

[47] R. H. Elabd and A. J. A. Al-Gburi, "Design and Optimization of a Circular Ring-Shaped UWB Fractal Antenna for Wireless Multi-Band Applications Using Particle Swarm Optimization," in Progress in Electromagnetics Research B, vol. 106, pp. 101–112, 2024, DOI: 10.2528/PIERB24033002

[48] A. Benkhadda, A. Najid, A. El Aroudi, and A. El Hamichi, "A Compact Tri-Wideband Hexagonal Sierpinski Fractal Antenna for Wireless Applications," in Fractal and Fractional, vol. 7, no. 2, pp. 1–18, 2023, DOI: 10.3390/fractalfract7020115

[49] A. Raj and B. Mandal, "Design and Analysis of Sierpinski Fractal Antennas for Millimeter-Wave 5G and Ground-Based Radio Navigation Applications," in *Transactions on Emerging Telecommunication Technologies*, vol. 170, pp. 154123, 2024, DOI: 10.1002/ett.70001

[50] A. J. Al-Gburi, H. A. Abdulrazzaq, A. T. Almuhanna, and S. A. Mahdi, "Miniaturized Tri-Wideband Sierpinski Hexagonal Fractal Antenna for Wireless Communication Applications," in *Fractal Fract*, vol. 7, no. 2, pp. 1–15, 2023, DOI: 10.3390/fractalfract7020115

[51] A. K. Vallappil, et al., "Minkowski–Sierpinski Fractal Structure-Inspired 2 × 2 Antenna Array for Use in Next-Generation Wireless Systems," in *Fractal Fract*, vol. 7, no. 2, pp. 1–12, 2023, DOI: 10.3390/fractalfract7020158

[52] A. K. Sohi, A. Kaur, "A Complementary Sierpinski Gasket Fractal Antenna Array Integrated with a Complementary Archimedean Defected Ground Structure for portable 4G/5G UWB MIMO Communication Devices," in *Microwave and Optical Technology Letters*, vol. 62, no. 7, pp. 2595–2605, 2020, DOI: 10.1002/mop.32356

[53] M. Marzouk, Y. Rhazi, I. H. Nejdi, F.-E. Zerrad, M. Saih, S. Ahmad, A. Ghaffar, and M. Hussein, "Ultra-Wideband Compact Fractal Antenna for WiMAX, WLAN, C and X Band Applications," in *Sensors*, vol. 23, no. 9, 2023, DOI: 10.3390/s23094254

[54] Y. K. Choukiker and S. K. Behera, "Modified Sierpinski Square Fractal Antenna Covering Ultra-Wide Band Application with Band Notch Characteristics," in *IET Microwaves, Antennas and Propagation*, vol. 8, no. 7, pp. 589–596, 2014, DOI: 10.1049/iet-map.2013.0235